Article

Geochemical, Geotechnical, and Microbiological Changes in Mg/Ca Bentonite after Thermal Loading at 150 °C

Vlastislav Kašpar [1,2,*], Šárka Šachlová [1], Eva Hofmanová [1], Bára Komárková [3,4], Václava Havlová [1], Claudia Aparicio [5], Kateřina Černá [6], Deepa Bartak [6] and Veronika Hlaváčková [6]

1   Fuel Cycle Chemistry Department, ÚJV Řež, a. s., Hlavní 130, 250 68 Husinec, Czech Republic; sarka.sachlova@ujv.cz (Š.Š.); eva.hofmanova@ujv.cz (E.H.); vaclava.havlova@ujv.cz (V.H.)
2   Department of Water Landscape Conservation, Faculty of Civil Engineering, Czech Technical University in Prague, Thákurova 7, 166 29 Praha 6, Czech Republic
3   Centre of Instrumental Techniques, Institute of Inorganic Chemistry of the Czech Academy of Sciences, Husinec-Řež 1001, 250 68 Husinec, Czech Republic; komarkova@iic.cas.cz
4   Department of Chemistry, Faculty of Science, University of Ostrava, 30. dubna 22, 701 03 Ostrava, Czech Republic
5   Department Material and Mechanical Properties, Centrum výzkumu Řež s.r.o., Hlavní 130, 250 68 Husinec, Czech Republic; claudia.aparicio@cvrez.cz
6   Institute for Nanomaterials, Advanced Technologies and Innovation, Technical University of Liberec, Bendlova 7, 460 01 Liberec, Czech Republic; katerina.cerna1@tul.cz (K.Č.); deepa.bartak@tul.cz (D.B.); veronika.hlavackova@tul.cz (V.H.)
*   Correspondence: vlastislav.kaspar@ujv.cz; Tel.: +420-266172087

Abstract: Bentonite buffers at temperatures beyond 100 °C could reduce the amount of high-level radioactive waste in a deep geological repository. However, it is necessary to demonstrate that the buffer surrounding the canisters withstands such elevated temperatures, while maintaining its safety functions (regarding long-term performance). For this reason, an experiment with thermal loading of bentonite powder at 150 °C was arranged. The paper presents changes that the Czech Mg/Ca bentonite underwent during heating for one year. These changes were examined by X-ray diffraction (XRD), thermal analysis with evolved gas analysis (TA-EGA), aqueous leachates, Cs sorption, cation exchange capacity (CEC), specific surface area (SSA), free swelling, saturated hydraulic conductivity, water retention curves (WRC), quantitative polymerase chain reaction (qPCR), and next-generation sequencing (NGS). It was concluded that montmorillonite was partially altered, in terms of the magnitude of the surface charge density of montmorillonite particles, based on the measurement interpretations of CEC, SSA, and Cs sorption. Montmorillonite alteration towards low- or non-swelling clay structures corresponded well to significantly lower swelling ability and water uptake ability, and higher saturated hydraulic conductivity of thermally loaded samples. Microbial survivability decreased with the thermal loading time, but it was not completely diminished, even in samples heated for one year.

Keywords: magnesium bentonite; radioactive waste disposal; thermal loading; montmorillonite content; thermal analysis with evolved gas analysis; cation exchange capacity; specific surface area; saturated hydraulic conductivity; water retention curves; microbial survivability

1. Introduction

Spent nuclear fuel (SNF) generates significant heat via radioactive decay. After a period of aboveground cooling, a deep geological repository (DGR) is considered the only suitable way to dispose of such high-level radioactive waste. For many DGR concepts, the temperature on the interface between disposal canisters and bentonite buffer is typically designed to be lower than 100 °C. If a higher temperature is allowed (beyond 100 °C), the cooling and storage period could shorten, or more SNF assemblies could be loaded in the disposal canister. Both would positively affect the economy of radioactive waste

disposal, especially when considering size optimisation [1]. However, possible changes in DGR designs must be justified, by proving that the performance targets for the engineered barrier safety functions are fulfilled, even at an elevated temperature, and confirming that the repository ensures post-closure radiation safety.

The thermal criterion of not exceeding a buffer peak temperature of 100 °C was chosen to avoid bentonite alteration [2]. Alteration here refers to mineral transformations of montmorillonite, leading to low- or non-swelling clay structures, which may not meet the buffer safety criteria for swelling pressure and hydraulic conductivity. Several possible processes, such as atomic substitutions (eventually, iron reduction/oxidation) in the mineral structure, layer charge redistribution, balanced by the compensating cations and congruent dissolution, are involved in the montmorillonite transformation [2]. The main alteration processes involve the transformation to illite/montmorillonite mixed layers, illite, beidellite, saponite, or chlorite [2,3].

Moreover, bentonite soluble components dissolve under hydrothermal conditions and the solutes may interact with silica released by the montmorillonite transformation, resulting in precipitation of new Si phases (so-called cementation), also contributing to a reduction of buffer plasticity and an increase of hydraulic conductivity [2,3]. Cementation can also be caused by non-Si compounds (e.g., sulphate and carbonate minerals), showing increased stability at higher temperatures [3].

Based on the critical review of the performance of the bentonite barrier, at temperatures beyond 100 °C, Wersin et al. [3] supported the idea of raising the thermal criterion to 120 °C; they identified higher thermal stability of bentonite under dry conditions (up to 300 °C) and noted the scarce data on hydraulic and mechanical properties of heat-exposed bentonites. The highest temperature yet applied in-situ was in the ABM5 experiment at Äspö Hard Rock Laboratory (Sweden). Temperatures up to 250 °C were achieved at the steel heater interface with compacted bentonites [1,4]. No significantly different chemical and mineralogical reactions were observed compared to the previous ABM tests or similar tests performed in the temperature range of 90–130 °C. In this test, the extent of magnesium enrichment, in the vicinity of the heater, observed in many large-scale tests, was small [4]. No data on the characterisation of bentonites from the ABM5 experiment from the geotechnical point of view is yet available. Complete ABM experiments provided geotechnical data for MX-80, Asha 505, Deponit CAN, and Friedland clay. Slightly lower swelling pressure was determined for heat-exposed materials Asha 505, Deponit CAN, and Friedland clay. No changes in hydraulic conductivities between the above reference and in-situ exposed materials were observed [5–7].

The influence of higher temperatures on bentonite performance and the lack of data from the thermo-hydro-mechanical (THM) behaviour of clay-based materials led to identifying this topic as a high priority subject within the framework of the EURAD project—WP7 HITEC. In general, two approaches are used to investigate thermally induced effects on clay-based materials.

The first approach examined HM properties at different temperatures. Geotechnical parameters of water-saturated compacted bentonites (FEBEX, MX-80, and Korean Ca-bentonite) were determined at temperatures ranging from 20 to 150 °C [8–12]. Decreasing swelling pressure and suction pressure and increasing hydraulic conductivity with temperature were assigned to the temperature-dependent water properties and physico-chemical interactions of water at the microscopic level [9]. However, once corrected for temperature-dependent water density and viscosity, the intrinsic permeability was not significantly temperature dependent [11,12]. This approach demonstrates buffer safety functions (namely swelling pressure and hydraulic conductivity) at all thermal stages within the DGR evolution.

In the second approach, the material property changes of preheated material were analysed. The material was mainly provided from in-situ experiments, which were designed to simulate the heat released from waste canisters containing radioactive waste. MX-80 bentonite, the "reference" one, and the one exposed to the temperature of 130 °C

at the copper heater in the form of parcel samples trimmed to the experimental cells, or re-compacted parcel samples to the original bulk density up to 2000 kg/m^3, was subjected to the determination of hydraulic conductivity (among other determinations). Slightly lower hydraulic conductivity in the trimmed samples in comparison to the re-compacted ones was observed. However, no significant difference between samples from different positions (warm, cool) in the parcel was observed; therefore, the decrease could not be related to temperature gradients [13]. A mixture of FoCa clay with 35 wt.% sand and 5 wt.% graphite was used in OPHELIE mock-up experiment where a temperature up to 140 °C was maintained for 4.5 years [14]. Slightly higher hydraulic conductivity of exposed material was determined. The authors explain this fact with thermally induced changes of the sample microstructure. An increase in intermediate pore sizes within the samples with temperature, which caused an increase in water and the cross-sectional area available for water to flow, was indicated by mercury intrusion porosimetry. Moreover, water retention curves were determined. Thermally loaded samples showed lower water retention capacity than the initial ones for the lower suction levels. For suction pressure over 150 MPa, no difference was observed. Thermally loaded samples showed less pronounced hysteresis than the initial ones, which was also attributed to the microstructural changes mentioned above [14].

Natural clay materials (e.g., bentonites) also represent an important source of indigenous microorganisms [5,15]. The microbial activity might negatively affect the long-term safety of DGR as it can result in microbiologically influenced corrosion of the canister and possibly alter the bentonite mineralogy [16,17]. Microbial survival and growth are generally inhibited by thermal and radiation performance after deposition of the canister [17]. However, bacterial endospores that are microbial survival forms with reduced water content, and undetectable metabolic activities, can tolerate adverse environmental conditions, such as desiccation, wet and dry heat (above 100 °C), and UV and gamma irradiation for extended periods [18,19]. Several studies in the bentonite environment have also demonstrated microbial survivability. Masurat et al. [20,21] found a loss of sulphate-reducing bacteria (SRB) viability after loading MX-80 bentonite at 120 °C for 20 h. However, another experiment with even more prolonged heating for one week failed to eradicate SRB [22]. Similarly, the presence of indigenous SRB, which survived heat loading of Boom Clay at 120 °C for 48 h, was reported [23]. Eleven compacted bentonites were exposed to groundwater saturation and high temperatures (90–130 °C) in the in-situ experiment—Alternative Buffer Material at the Äspö Hard Rock Laboratory—for approximately one year. Microbial analyses of three bentonites within the first test package showed a detrimental effect of heat on bacterial activity. The bacterial growth was scarce; only mesophilic aerobic heterotrophs in the range of 10^2–10^3 g^{-1} wet weight were cultivated [5].

It can be presumed that, during the early stage of disposal, when the buffer is exposed to an elevated temperature induced by the radioactive waste and, concurrently, is not yet saturated by the groundwater, the microbial activity would be insignificant. However, the safety functions of bentonite may be affected at this stage. Therefore, it is crucial to identify potential changes in the safety functions of bentonite when exposed to elevated temperatures. This work explores Czech Mg/Ca bentonite before and after medium-term thermal loading at 150 °C in a powder state. Several techniques and methods were chosen for geochemical and geotechnical characterisation (e.g., XRD, TA-EGA, aqueous leachates, CEC, SSA, free swelling, saturated hydraulic conductivity, WRC). In addition, microbiological methods were used to investigate bacterial survivability in thermally loaded bentonite and the ability to regenerate from spores in favourable cultivation conditions.

2. Materials and Methods

2.1. Bentonite Powder

It is anticipated that Czech bentonites will be used in the construction of engineered barriers in the future Czech DGR project [24]. For this study, a commercial bentonite product originating from the Černý vrch deposit (Keramost PLC, Most, Czech Republic)

was chosen. Bentonite Černý vrch (BCV) is dominated by montmorillonite, with prevailing divalent exchangeable cations (mainly magnesium). Basic characteristics of the BCV bentonite were summarised in an HITEC SotA report [1].

Since December 2019, approximately 10 kg of bentonite powder in open stainless-steel vessels have been exposed to a 150 °C temperature in a heating chamber (Binder, Tuttlingen, Germany). This set-up was designed to simulate an early post-closure state of the DGR; when radioactive decay generates a significant amount of heat, oxygen is still available, and the buffer is not saturated by the groundwater. Overall, thermal loading of bentonite powder was planned for two years. This paper deals with the characterisation of the initial BCV bentonite (denoted as BCV_IN) and two subsamples taken from the thermally loaded bentonite after a year and a half (denoted as BCV_0.5_y and BCV_1.0_y, respectively).

The first sampling revealed a colour change of bentonite on the surface, from light brown to dark brown (see Figure 1). The thin surface layer was sampled as a separate sample. The same procedure was then followed for the second sampling, after one year. This paper only focuses on the characterisation of the bentonite powder beneath the thin surface layer. This sample defines the barrier properties and allows evaluating the impact of the thermal loading. The effect of the potential thermally induced surface buffer layer near the containers on the DGR is expected to be negligible (regarding long-term safety) due to the minimal thickness. However, future research should focus on the properties of the thermally induced surface layer and the extent to which it will form in a compacted state.

(a)	(b)

Figure 1. (**a**) Thermal loading of bentonite powder in open vessels, and (**b**) visible colour change from light brown to dark brown at the powder surface observed during sampling.

2.2. Geochemical Characterisation

Bentonite powder samples were subjected to various determinations, providing insight into geochemical properties, such as the composition of major minerals, the identification of gaseous products evolved upon heating, or soluble phases released on contact with water. Cation exchange capacity (CEC), specific surface area (SSA), and caesium sorption determination were selected to characterise the clay component in bentonite.

Powder X-ray diffractometry (XRD) was conducted on an Empyrean third generation diffractometer (Malvern Panalytical B.V., Almelo, Netherlands) with the following measurement conditions: Co-K$_\alpha$ radiation, a PIXcel3D detector, a range 3.5–105° 2θ, a step of 0.026° 2θ, and a total counting time of 5.25 h. Randomly oriented powder mounts (with inner ZnO standard) and clay fraction (oriented specimens) were analysed. Minerals were identified using HighScore Plus version 4.8 (Malvern Panalytical B.V., Almelo, The Netherlands) software and PDF-4+ 2020 database. Quantitative analysis was performed using a graphical user interface Profex v.4.2.1 (Nicola Döbelin, Solothurn, Switzerland) [25].

Thermal analysis with evolved gas analysis (TA-EGA) was performed on SetSys Evolution's apparatus (Setaram, Calurie-et-Curie, France). The weight of the as-received samples was approximately 10 mg. Thermal degradations of bentonites were studied

under an argon atmosphere (flow of 60 mL/min) in α-Al_2O_3 crucible. The heating rate was set to 10 °C/min in the temperature range of 30–1000 °C. Gases that evolved during heating were analysed with a quadrupole mass spectrometer QMG 700 (Pfeiffer Vacuum, Asslar, Germany) connected to a thermal analyser through a Supersonic System (Setaram, Calurie-et-Curie, France). Specific fragments corresponding to water, carbon dioxide, and sulphur oxides, were recorded.

The soluble salts were identified based on aqueous leachates. The dried (105 °C) samples were contacted with deionised water (40 mL) at three solid-to-liquid ratios for seven days. The suspensions were centrifuged, and supernatants were filtered using a 0.2 μm syringe filter. The main cations in the filtrates were analysed using atomic absorption spectrometer SavantAA (GBC Scientific Equipment, Braeside, Australia). The total alkalinity of the filtrates was determined by potentiometric titration using Titralab TIM800 (Radiometer Analytical, Loveland, USA). The concentrations of sulphates, chlorides, and fluorides were determined by ion chromatography (ALS Global, Prague, Czech Republic).

The highest solid-to-liquid ratio was also tested for caesium sorption. After seven days of shaking, the bentonite suspension of 200 g/L, aliquots of CsCl spiked with ^{134}Cs were added and interacted for another seven days. Two initial caesium concentrations of spiking aliquots (0.001 mol/L and 6.4 mol/L) were chosen. Aliquots from supernatants, separated by centrifugation, were determined for ^{134}Cs activity on gamma counter 1480 Wizard 3 (Perkin Elmer, Waltham, USA). Blank samples (without solid phase) were prepared and processed in the same way to evaluate the distribution coefficient of Cs. Each sorption experiment under the given conditions was performed in duplicate.

The CEC and exchangeable cations were determined by the Cu(II)-triethylenetetramine (Cu-trien) method [26,27]. Cu-trien (0.01 mol/L) was mixed with dried (105 °C) samples in the solid-to-liquid ratio of 25 g/L. After interaction for 30 min, the suspensions were centrifuged, and supernatants were analysed. The Cu^{2+} concentration was determined by UV/Vis spectrophotometer Specord 205 (Analytik Jena, Jena, Germany). The concentration of displaced cations (Na^+, K^+, Ca^{2+}, and Mg^{2+}) was determined by atomic absorption spectrometer SavantAA (GBC Scientific Equipment, Braeside, Australia). Two values of cation exchange capacity were derived: CEC_{Vis} from copper depletion and CEC_{SUM} by summing equivalent concentrations of displaced cations.

The specific surface area (SSA) was determined based on the sorption of ethylene glycol monoethyl ether (EGME) [28,29]. Moreover, 1 g of bentonite powder (dried at 105 °C) was mixed with 2 mL of EGME and equilibrated in a desiccator with $CaCl_2$-EGME solvate. The applied procedure [30] consisted of regular desiccator evacuation and monitoring of the samples until a constant weight was reached. The SSA was derived from the mass ratio of adsorbed EGME and dried bentonite sample.

2.3. Geotechnical Characterisation

Free swelling tests, determination of water retention curves (WRC), and saturated hydraulic conductivity were selected for geotechnical characterisation. Free swelling tests were performed with 10 mL deionised water and 0.6 g powders (previously dried at 105 °C). This solid-to-liquid ratio allows a better determination of the swell index in graduated cylinders for low swelling materials (such as Ca- and Mg-bentonites), highlighting the differences between the input and the thermally loaded bentonite samples. The standard ratio of 0.02 g/L [31] did not allow the determination of the swell index nor the comparison between the samples.

Bentonite dry densities of 1400, 1600, and 1800 kg/m^3 were chosen for determining saturated hydraulic conductivity and WRC. Bentonite powder was compacted in the cylindrical space of a cell body (diameter of 30 mm, thickness of 15 mm) using a hydraulic press MEGA 11-300 DM1S (FORM+TEST Seidner & Co., Riedlingen, Germany). In the WRC experiments, a hole was drilled for placing a wireless sensor (diameter of 17 mm, depth of 6 mm). The compacted sample was closed with end plates composed of stainless

steel fabrics placed on the carbon composite percolator [32]. Three-quarter section views of the experimental cells are shown in Figure 2.

(**a**) (**b**)

Figure 2. Experimental cell set-up for measuring (**a**) saturated hydraulic conductivity and (**b**) water retention curves.

Saturated hydraulic conductivity of compacted bentonite was determined according to ISO 17892-11:2019. The cells were placed into a desiccator filled with deionised water. The desiccator was regularly vacuumed for at least two weeks. After water saturation, the cell was connected via pressure hoses to the assembly for measuring saturated hydraulic conductivity consisted of an input and output pressure controller (HPDPC and ELDPC, GDS Instruments, Hook, UK). Hydraulic heads of 5, 8, and 10 MPa were applied for the dry density of 1400, 1600, and 1800 kg/m^3, respectively. The experiment was terminated when a steady-state water flow was reached, and the output water flow equalled the input water flow. The cell was dismantled, and the actual dry density was determined. The hydraulic conductivity was calculated according to Darcy's law and converted to a referential temperature of 10 °C according to the ISO standard.

The block/sensor method [33] was used to determine WRC. A wireless sensor with its internal memory, Hygrochron iButton (Maxim Integrated, San Jose, CA, USA), was applied for measuring relative humidity and temperature inside the compacted sample exposed to saturated air with water vapour inside a desiccator filled with water. The cell was regularly weighed until a constant mass was reached. When constant mass was achieved, the cells were dismantled and the sensors removed. The measured data of relative humidity and temperature were used to calculate the suction pressure according to the Kelvin equation for each time interval. WRC were then constructed as a dependence between suction pressure and gravimetric water content.

2.4. Microbiological Characterisation

Cultivation of bentonite suspensions in an anaerobic atmosphere rich in H_2, with a subsequent molecular genetic analysis, was used for studying microbial survivability in bentonite samples exposed to thermal loading. The bentonite suspensions were prepared from 2 g of naturally wet bentonite powders, mixed with 10 mL sterile Milli-Q water. Samples were incubated in an anaerobic workstation (Don Whitley Scientific, Bingley, United Kingdom) under an atmosphere containing 94% Ar and 6% H_2 at room temperature. Suspensions were sampled at three different cultivation times, immediately after phases mixing (0 d), after 14 and 28 days, and kept in a freezer until DNA isolation. Zero-point (0 d) samples and BCV_IN samples were prepared in duplicate, whereas the heat-loaded samples in triplicate.

The DNA from the bentonite samples was extracted by DNeasy® PowerMax® Soil Kit (QIAGEN, Germantown, TN, USA) according to the manufacturer's protocol. The extracted DNA was concentrated and purified by the DNA Clean & Concentrator Kit (Zymo Research, Irvine, CA, USA) and quantified by a Qubit 2.0 fluorometer (Life Technologies, Carlsbad, CA, USA). One background kit control without the sample was co-extracted

together with samples in each DNA extraction batch to see the laboratory background and possible contaminations resulting from the kit or the laboratory. The extracted DNA was used to describe the microbial composition in the samples (16S rDNA amplicon sequencing, NGS) and for the relative quantification of microbial biomass in the samples (16S rDNA quantitative PCR). For these DNA-based analyses, protocols similar to [34] were followed.

3. Results

3.1. XRD

The bulk mineralogical composition of the bentonites is shown in Table 1. Bentonite samples are dominated by montmorillonite (d_{060} ~ 1.50 Å), accompanied mainly by quartz and kaolinite. According to the position of the basal diffraction of the untreated sample (d_{001} ~ 14.9 Å), Ca-montmorillonite was identified. The presence of saponite and nontronite was excluded in all samples based on an absence of d_{060} spacing at 1.52 Å. Of all remaining crystalline phases, illite, goethite, anatase, calcite, aragonite, siderite, and sanidine were quantified in amount <5 wt.%. Analcime, ankerite, and augite were detected in very small amounts (bellow quantification limit). Measurements of as-received samples with ZnO inner standard indicated a reduction of amorphous phases in thermally loaded samples. Therefore, depending on the quantification method used, montmorillonite content decreased slightly or remained almost unchanged in thermally loaded samples. No significant bentonite alteration in terms of mineral transformation can be established considering the uncertainties of the XRD method, especially when dealing with clay minerals and trace minerals. However, basal diffraction of montmorillonite progressively disappeared, indicating increasing disorder of the montmorillonite layers and dehydration connected to the thermal loading.

Table 1. Semiquantitative XRD analysis of randomly oriented powder mounts (wt.%); bql—below quantification limit, nd—not detected.

Phases	BCV_IN	BCV_0.5_y	BCV_1.0_y
Montmorillonite	72	68	71
Quartz	10	10	10
Kaolinite-1A	6	8	6
Illite-2M1	2	3	3
Sanidine	2	3	3
Goethite [1]	3	3	3
Anatase	2	2	2
Calcite	1	1	1
Aragonite	1	1	1
Siderite	1	1	bql
Ankerite	bql	bql	bql
Augite	nd	bql	nd
Analcime	nd	bql	bql
Total	100	100	100

[1] Amount of goethite may be underestimated due to the small size of crystallites.

3.2. TA-EGA

The results of simultaneously performed thermogravimetry (TG) and differential thermal analysis (DTA) supplemented with mass spectrometry identification of evolved gases can be seen in Figure 3. Variability of endothermic and exothermic processes in DTA curves suggests a complex composition of BVC bentonite. Four major mass losses were identified from the derivative thermogravimetric (dTG) curves: at approximately 30–200, 200–300, 300–600, and 600–800 °C. Water-related mass losses were found for the first three processes. A shift of 240 °C peak of BCV_IN to higher temperatures was observed for thermally loaded samples. The same shift was also observed in the EGA curves of evolved water. Another difference in the EGA curve for CO_2 can be seen at 105 °C and in the region

of 350–550 °C. A very low signal for SO_2 was registered around 800 °C, decreasing in order: BCV_IN > BCV_0.5_y > BCV_1.0_y.

3.3. Aqueous Leachates

Interaction of bentonite samples with deionised water at three solid-to-liquid ratios resulted in the leachate composition of studied ions are presented in Table 2. The dominant aqueous species were Na^+ and HCO_3^-. The HCO_3^- source is the dissolution of carbonate phases, which are abundant in BCV bentonite. Dissolution of carbonate phases is followed by cation exchange reactions releasing cations, particularly Na^+, into the leachate [35,36]. The concentrations of all ions increase with increasing bentonite content. All ion concentrations, except for chloride and sulphate, also increase with the heating period of bentonite powder. It follows that the reactivity of soluble phases has changed. The thermal loading somehow affected the bentonite, possibly in terms of mineral transformation or recrystallisation. More considerable changes in bentonite/water reactivity were detected in the first heating period.

Differences in leachable cation concentrations between the heated and input samples were found mostly for calcium, then potassium and magnesium. The released Na^+ concentration is comparable for all materials corresponding to the lowest capability of sodium to compete at montmorillonite exchange sites. Powder heating at 150 °C resulted in the most pronounced increase in leachable fluoride concentrations, up to 2.2 times. The bicarbonate concentration in leachates from the heated samples was up to 1.6 times higher than from the BCV_IN sample. The concentration of leachable SO_4^{2-} and Cl^-, on the other hand, decreased with the thermal loading of bentonite powders, indicating a decrease in the solubility of the chloride and sulphate phases.

(a)

(b)

Figure 3. *Cont.*

(**c**)

(**d**)
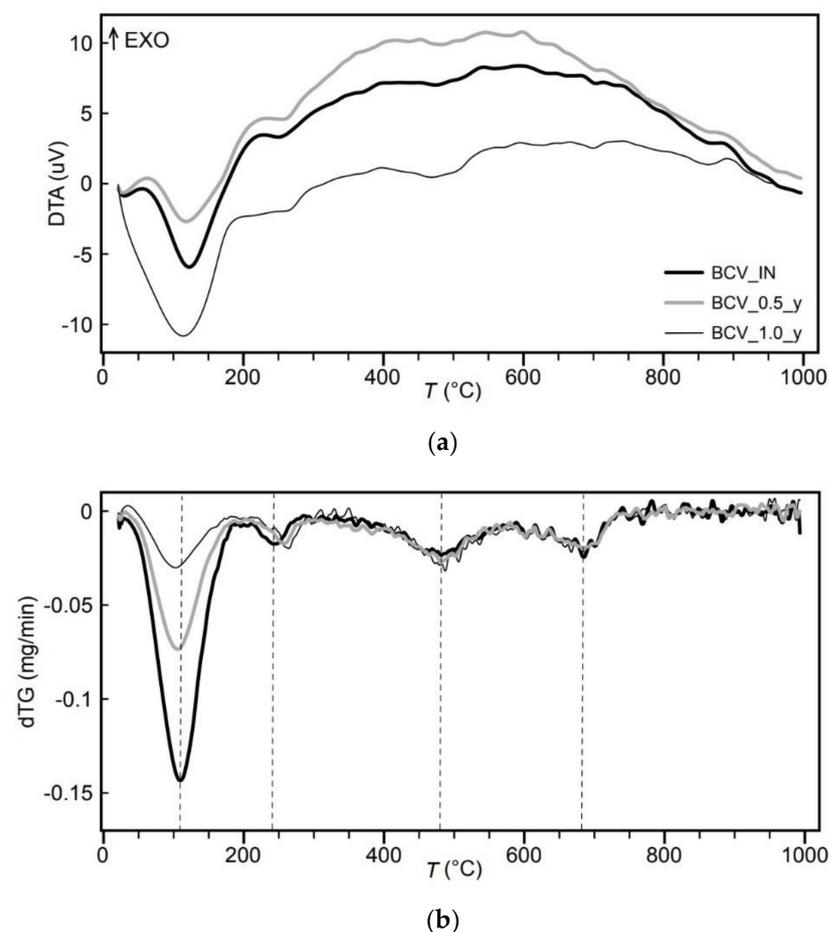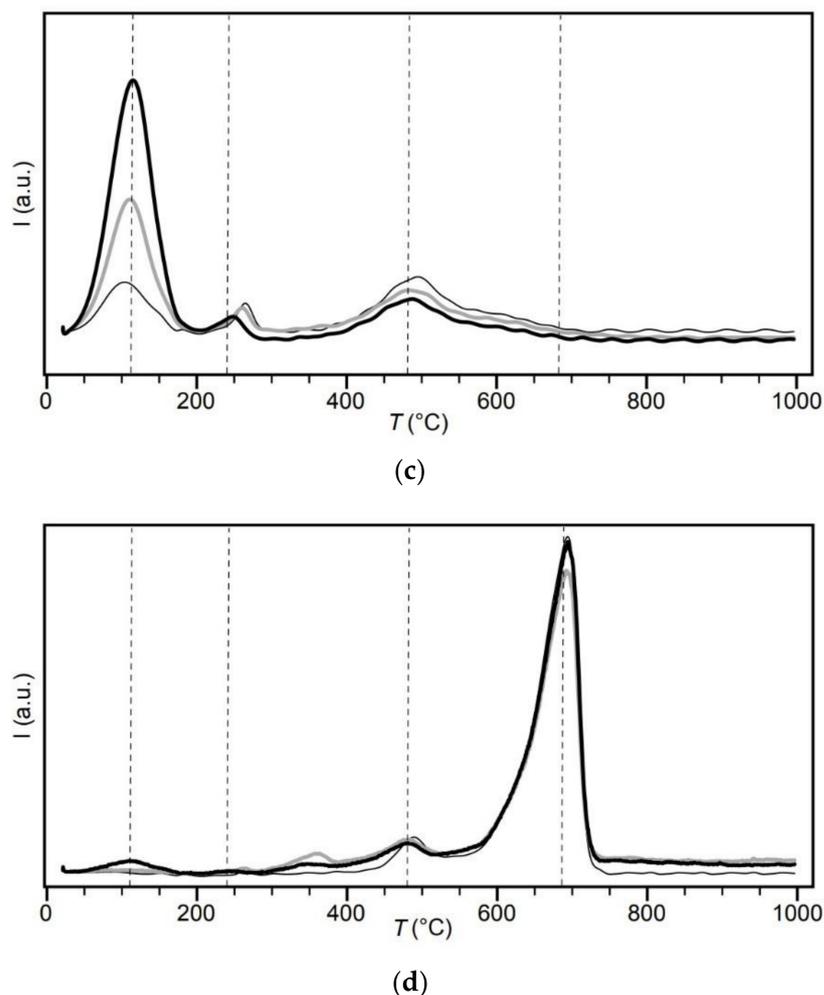
Figure 3. TA-EGA. Differential thermal analysis (**a**), derivative thermogravimetry curves (**b**), EGA curves for water (**c**), and CO_2 (**d**) of the powder samples.

Table 2. Aqueous leachates data for the studied BCV samples at three different solid-to-liquid ratios.

mmol/L	IN 25 g/L	0.5_y 25 g/L	1.0_y 25 g/L	IN 112.5 g/L	0.5_y 112.5 g/L	1.0_y 112.5 g/L	IN 200 g/L	0.5_y 200 g/L	1.0_y 200 g/L
Na^+	1.4	1.5	1.5	3.8	4.1	4.1	4.9	5.5	5.9
K^+	0.13	0.26	0.32	0.26	0.51	0.60	0.33	0.62	0.81
Ca^{2+}	0.061	0.19	0.24	0.10	0.22	0.26	0.13	0.27	0.33
Mg^{2+}	0.11	0.23	0.22	0.23	0.36	0.33	0.29	0.49	0.49
HCO_3^-	1.7	2.4	2.6	3.8	5.1	5.2	4.8	6.6	7.3
SO_4^{2-}	0.065	0.062	0.060	0.25	0.23	0.21	0.44	0.36	0.35
Cl^-	0.011	0.009	0.009	0.032	0.024	0.021	0.053	0.040	0.040
F^-	0.028	0.061	0.059	0.089	0.14	0.12	0.097	0.16	0.14

3.4. Caesium Sorption

The used methodology of sorption experiments covered two extremes of the Cs concentration range: 0.0008 and 62 mmol/L of the initial carrier concentration, resulting in the distribution coefficients presented in Table 3. In both cases, the lowest decrease in Cs concentration was observed in the supernatant of the BCV_1.0_y sample. This sample contained the largest amount of leachable ions that may compete in the sorption process. The lowest K_d for BCV_1.0_y could be caused by cation competition or reflects an alteration of the sorption sites. Cs sorption experiments at a wide concentration range of carrier and

competing cations on bentonites, smectite-rich clays, and illite-rich clay identified K^+ as the major competitive cation, followed by Ca^{2+} and finally by Na^+ at low Cs concentration [37]. In our experiments, the main competing cation was Na^+; the concentrations of other competing cations (see Table 2) were much lower than those affecting the Cs sorption process [37]. Competition of Cs^+ with leachable cations for sorption sites can also be ruled out in experiments with the applied high concentration, where caesium represents the dominant cation. Decreasing K_d values thus indicate a reduction in the sorption sites for Cs when bentonite powder was thermally loaded.

Table 3. Caesium distribution coefficients K_d at two different carrier concentrations (low~0.0008 mmol/L Cs, high~62 mmol/L Cs).

Bentonite Sample	K_d_low	K_d_high
	(mL/g)	
BCV_IN	5322 ± 533	29.28 ± 0.66
BCV_0.5_y	4478 ± 379	28.66 ± 0.65
BCV_1.0_y	2621 ± 164	27.73 ± 0.62

3.5. Cation Exchange Capacity, Specific Surface Area

The results of the CEC and SSA measurements are shown in Table 4. Both determined parameters decrease upon heating bentonite at 150 °C. While the SSA changed substantially after the first heating phase and then remained unaffected, the CEC steadily declined. The difference between the CEC_{SUM} and CEC_{Vis}, stating the proportion of minerals dissolution on the CEC value, increased. The rising amount of dissolved cations with the heating period of bentonite powder is consistent with the results of the aqueous leachates (see Table 2). Thus, the cation exchange experiment provides summary information about the cation replacements in the montmorillonite interlayers and the interaction of Cu-trien with the sample. Since these two phenomena cannot be discriminated, Figure 4 displays two variants of data processing. The first one does not allow the dissolution of any minerals or impurities. The concentration of displaced cations was related to the CEC_{SUM} value. The latter allows the same interaction of Cu-trien with the sample as water at the same solid-to-liquid ratio. The concentration of displaced cations was reduced by subtracting aqueous leachable cations at 25 g/L and was related to the reduced CEC_{SUM} value. No measurable amount of displaced iron in supernatants (in the CEC determination or in aqueous leachates) was detected.

Table 4. Cation exchange capacity and specific surface area data; *n* corresponds to the number of replicates.

Bentonite Sample	CEC_{Vis}	CEC_{SUM}	CEC_{SUM}-CEC_{Vis}	*n*	SSA	*n*
		(meq/100 g)			(m^2/g)	
BCV_IN	59.2 ± 1.4	62.6 ± 1.0	3.5 ± 1.7	13	468 ± 18	14
BCV_0.5_y	55.0 ± 1.5	59.2 ± 1.4	4.3 ± 2.1	12	436 ± 4	6
BCV_1.0_y	50.9 ± 1.0	58.3 ± 2.1	7.4 ± 2.3	9	435 ± 7	6

Depending on the CEC data processing and, thus, considering the dissolution reactions followed by the cation exchange reactions, the sodium population has significantly changed, because Na^+ was identified as the major water-leachable cation. Nevertheless, the trends in the exchangeable cations are identical regardless of the CEC data processing. Most of the exchangeable sites in BCV bentonite were occupied by magnesium and calcium. The exchangeable cations in thermally loaded samples varied with heating time. Magnesium proportion decreased at the expense of calcium and potassium; sodium remained unaffected upon heating.
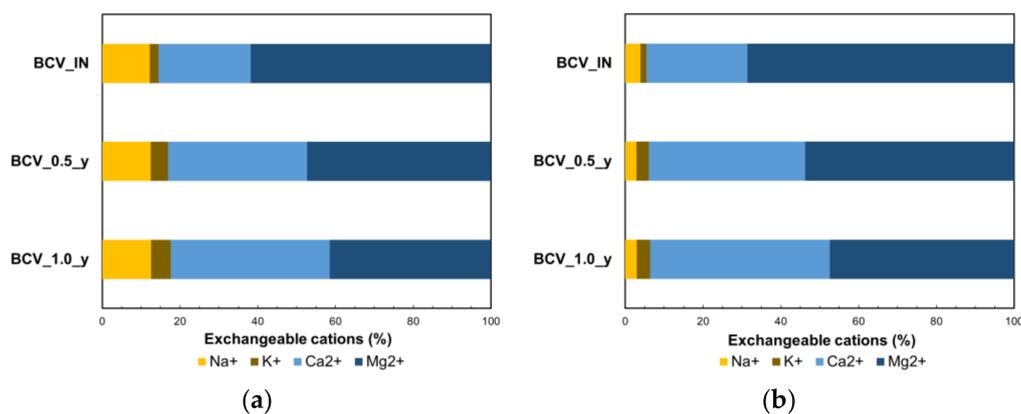
Figure 4. Exchangeable cations displaced by Cu-trien (**a**) and corrected by aqueous leachable cations (**b**).

3.6. Geotechnical Parameters

Free swelling of dried powders in water resulted in different volumes of swollen material. Steady-state volumes of BCV_IN, BCV_0.5_y, and BCV_1.0_y were 4.8, 2.1, and 1.8 mL, respectively.

Table 5 presents the results of saturated hydraulic conductivity measurements. Thermally loaded samples showed higher saturated hydraulic conductivities; the longer the loading period, the higher the saturated hydraulic conductivity. For all dry densities, saturated hydraulic conductivity increased ca 1.3 times when thermally loaded for half a year and ca 1.6 times when thermally loaded for one year.

Table 5. Saturated hydraulic conductivity k_{10} data for studied samples at actual bentonite dry density ρ_d.

Bentonite Sample	ρ_d (kg/m^3)	k_{10} (m/s)
	1420	$2.8 \cdot 10^{-13}$
BCV_IN	1581	$1.0 \cdot 10^{-13}$
	1784	$4.1 \cdot 10^{-14}$
	1427	$3.7 \cdot 10^{-13}$
BCV_0.5_y	1605	$1.3 \cdot 10^{-13}$
	1730	$6.3 \cdot 10^{-14}$
	1434	$4.1 \cdot 10^{-13}$
BCV_1.0_y	1587	$1.6 \cdot 10^{-13}$
	1773	$6.1 \cdot 10^{-14}$

Wetting paths of water retention curves are displayed in Figure 5. It can be seen that the water retention ability of BCV bentonite decreases when thermally loaded. The biggest difference was found between the unloaded sample and the loaded ones; thermal loading time seemed to have a lesser impact. This trend was more significant for lower water content.
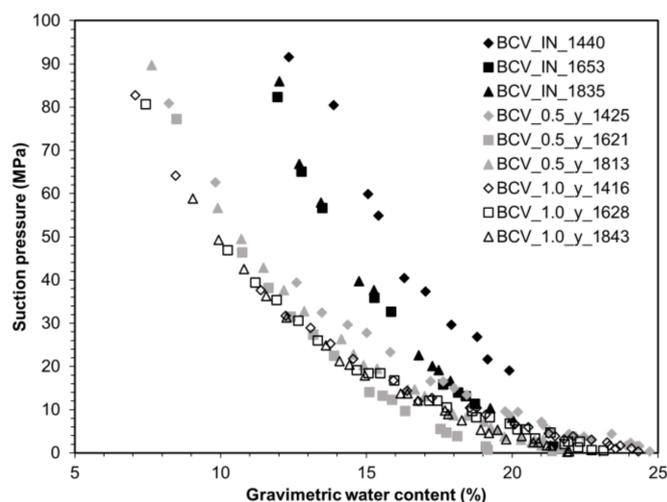
Figure 5. Water retention curves of compacted bentonite samples at given dry density (kg/m³).

3.7. Microbiological Characterisation

Generally, the DNA extraction resulted in very low DNA yields, as revealed by Qubit measurement. Therefore, the qPCR method by 16S rDNA marker was used to better distinguish between the samples and estimate the changes in gene copy number in the studied samples. The quantification cycle (Cq) values were related to the Cq values of freshly mixed suspensions (0 d) for each bentonite powder to quantify the magnitude of relative change in gene copy numbers. The PCR efficiency for the 16S rDNA marker was estimated beforehand by measuring the slope of curves constructed from a serial dilution of template DNA from several environmental samples. Relative quantification, displayed in Figure 6, showed an increase in the relative abundance of 16S rDNA copies in all samples after 28 days of cultivation in anaerobic conditions. The relative increase varied among samples. The highest relative increase was detected in BCV_0.5_y samples after 28 days of cultivation. A slightly lower relative increase was found for BCV_IN. The lowest relative increase in the gene copies was determined for BCV_1.0_y. Our data also show that 14 days of recovery time for restoring microbial activity from dormant stages is insufficient for most samples.
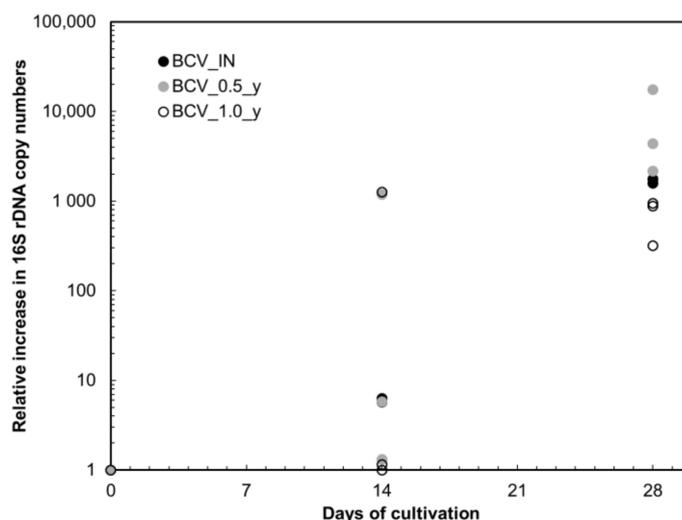
Figure 6. qPCR analysis of the 16S rDNA gene in anaerobically cultivated bentonite suspensions.

NGS sequencing technique enabled describing the microbial composition in the suspensions. The results of NGS sequencing (see Figure 7) were consistent with the qPCR

analyses. The low NGS signal was found for the studied samples with low 16S rDNA copy numbers and microbial abundance.
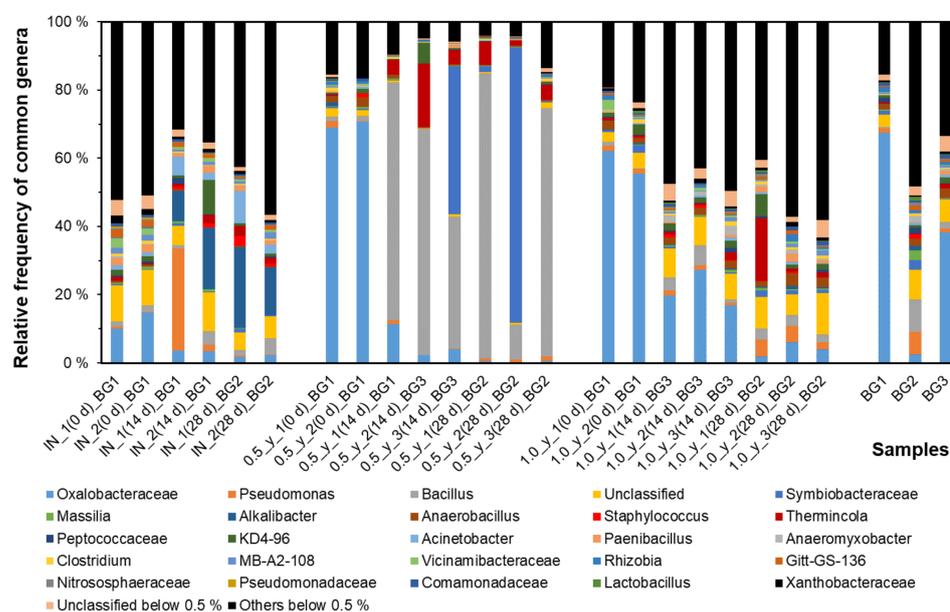
Figure 7. Relative abundance of detected microbial genera by NGS sequencing. The sample notation reflects the number from replicates, the cultivation time, and background (BG) controls co-extracted with each batch.

Various facultative anaerobic nitrate-reducing (NRB) genera such as *Alkalibacter, Acinetobacter, Bacillus, Pseudomonas, Paenibacillus, Symbiobacterium,* or *Massilia,* or iron-reducing (IRB) genus *Thermincola* were detected in BCV_IN samples. All of these genera are typical for Czech Mg/Ca bentonite [38]. Much lower genera diversity was found in the BCV_0.5_y samples. After 14 or 28 days of cultivation, the suspensions contained mostly the NRB genus *Bacillus* or the IRB genus *Thermincola*. In the samples 0.5_y_3(14 d)_BG3 and 0.5_y_2(28 d)_BG2, the presence of an unspecified bacterial clone from the family *Symbiobacteraceae* was detected. Sequencing of DNA from BCV_1.0_y samples resulted in poor NGS results. Only sample 1.0_y_1(28 d)_BG2 showed an increased frequency of the thermophilic genus *Thermincola* compared with the background controls (BG) co-extracted with the samples. This result indicates that, although the relative increase in 16S rDNA copy numbers in the BCV_1.0_y samples cultivated for 28 days was detected, this increase did not result in sufficiently high absolute gene copy numbers for successful NGS analysis. Microbial composition of all zero-point samples was very similar to the pattern detected in co-extracted background controls, which reflects their very low DNA content and lack of DNA signal similarly to the situation observed in 1.0_y samples. The only difference was observed in IN_1(0 d) and IN_2(0 d) samples, with lower proportion of *Oxalobacteraceae* family members compared to BG1 control. However, the relative frequencies of particular taxa are rather sensitive to several biases introduced during DNA extraction and PCR in low-DNA samples, and we consider the observed difference insignificant.

4. Discussion

The applied geochemical characterisation, targeting both the overall composition (in terms of mineralogy, thermolabile, and soluble phases) and the clay component, allowed investigating the effect of heating on individual components. The XRD analysis of BCV bentonite provided a substantial number of various phases, which may be affected by the exposition to the high temperatures, i.e., montmorillonite component, other clay minerals and non-clay minerals. Based on the XRD analysis, considering its uncertainties in detecting

variations in the structural chemical composition of clay minerals, it is not possible to deduce any significant mineral transformation upon heating.

The processes that the bentonite underwent up to 150 °C are indicated by the results of thermal analysis. Besides the apparent loss of water content in as-received samples, TA-EGA identified a release of CO_2 from the BCV_IN sample. Several CO_2-related mass losses were recorded when heating the bentonite samples to higher temperatures, up to 1000 °C. The CO_2 release can be attributed mainly to the carbonate phases, which XRD and aqueous leachates detected. Assigning peaks to given minerals is difficult due to superimpositions of double carbonates with calcite [39,40]. The presence of various carbonates in BCV might be reflected in the broad CO_2 peak at 600–800 °C. The main difference in thermal behaviour between BCV_IN and thermally loaded samples was found in the shift of H_2O and CO_2 peaks. These shifts, and release of CO_2 from the BCV_IN sample up to 150 °C, indicate some alteration process during bentonite heating. Altered reactivity of carbonates was also detected by aqueous leachates. A significantly higher concentration of leachable HCO_3^- from thermally loaded samples indicates an intense alteration of carbonate minerals, supported by the increased leaching of cations.

The impact of bentonite heating to 150 °C can also be inferred based on the leaching of fluorides, sulphates, and chlorides. A change, though to a minor extent, in sulphate content was also registered by TA-EGA. Nevertheless, no mineral phases containing fluorides, sulphates, and chlorides were detected by XRD. However, they may be present as impurities in minerals and/or in accessory amounts. For example, fluoride is commonly found in montmorillonites [5,41,42]. It can substitute the hydroxyl groups in the octahedral sheets [41]. The most significant increase in leachable concentration with exposure to elevated temperature has been determined for fluoride. An increased release of F⁻ into the solution might indicate montmorillonite lattice modification.

The effect of thermal loading on clay component was examined in detail using the determination of SSA and CEC and sorption experiments with caesium. The thermal loading caused a decrease in the SSA. A decrease in SSA upon heating up to 200 °C was also observed for Barmer bentonite [43]. A lower specific surface area may indicate recrystallisation of minerals or montmorillonite collapse. Lower amorphous phases in thermally loaded samples may indicate recrystallisation of minerals, often leading to textural coarsening. Coarsening then may facilitate the release of species when contacted with water. Higher leachable concentrations were found for thermally loaded samples. However, since EGME penetrates in the montmorillonite interlayers due to its polarity, the SSA decrease can be more attributed to the montmorillonite alteration than to recrystallisation of minerals.

Montmorillonite lattice modification in thermally loaded samples can be deduced from the experiments with selectively interacting cations (such as Cu-trien cation or Cs^+). The [134]Cs distribution coefficient at both studied carrier concentration decreased in the order: IN > 0.5_y > 1.0_y. The same trend was determined for the CEC determination with Cu-trien. Decreasing CEC due to extensive drying was observed in various bentonites and one illite/montmorillonite clay and was attributed to the type of exchangeable cations and their fixation [44]. Generally, the origin of the CEC is a permanent negative charge of montmorillonite clay layers due to isomorphous substitutions [45]. Altered reactivity of the applied selective cations, interacting by the cation exchange, clearly indicates a change in surface charge density of clay particles. Such a partial alteration can result in the formation of new phases (low-swelling or even non-swelling) at the expense of montmorillonite content.

To support the finding of reduced montmorillonite content, which could not be confirmed using XRD, data analysis of CEC, SSA was performed. The interlocking of SSA, CEC and smectite content is illustrated in Figure 8. Data selection (see Table 6) was mainly restricted by existing SSA values measured according to the EGME method. Previously published data were compared with the results from the current study. Five groups of bentonites can be distinguished corresponding to their smectite content. The lowest SSA and CEC values are typical for bentonites containing up to 50 wt.% of smectite. The highest

SSA and CEC values are typical for bentonites containing almost 100 wt.% of smectite. The CEC_{Vis} and SSA values of the BCV_IN sample correspond well with the correlation matching the group of bentonites containing 50–80 wt.% of smectite.
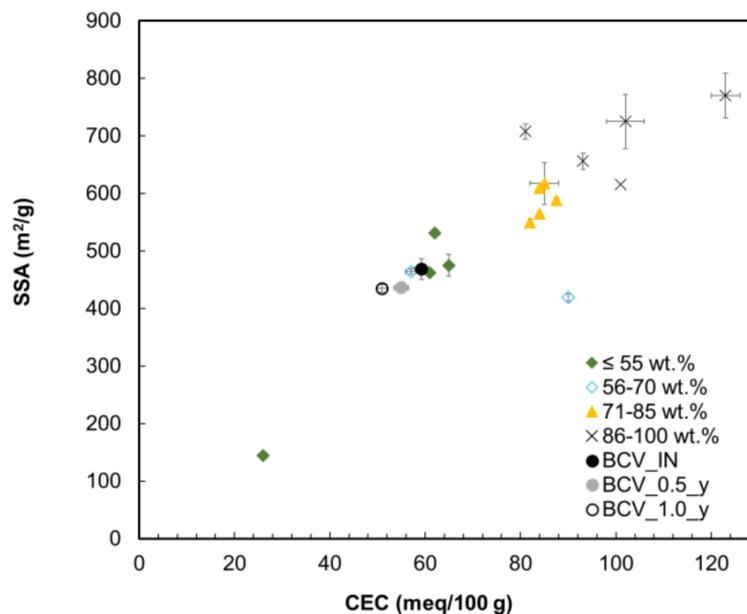
Figure 8. Correlation between CEC and SSA for various bentonites depending on their smectite content (wt.%).

Table 6. Data on smectite content, SSA and CEC of selected bentonites.

Bentonite Sample	Location	Smectite Content (wt.%)	SSA (m²/g)	CEC (meq/100 g)
SAz-1	Cheto (USA)	98 [46]	770 ± 39 [30]	123 ± 3 [47]
SWy-2	Wyoming (USA)	75 [46]	618 ± 37 [30]	85 ± 3 [47]
MX-80	Wyoming (USA)	81.3 [6]	610 ± 3 [6]	84 [6]
FEBEX	Cortijo de Archidona (Spain)	92 [48]	725 ± 47 [48]	102 ± 4 [48]
SPA 050	Cortijo de Archidona (Spain)	88 [37]	656 ± 14 [30]	93.1 [37]
SPA 04	Cortijo de Archidona (Spain)	75 [37]	588 ± 4 [30]	87.5 [37]
SPA 051	Cortijo de Archidona (Spain)	54 [37]	475 ± 19 [30]	64.9 [37]
Volclay KWK 20-80	Südchemie (Germany)	90 [49]	708 ± 14 [30]	81 [49]
Friedland clay	Friedland (Germany)	31.8 [6]	144 ± 2 [6]	26 [6]
Deponit CAN	Milos (Greece)	72.1 [6]	550 ± 5 [6]	82 [6]
Asha	Kutch (India)	67.1 [6]	419 ± 6 [6]	90 [6]
VSK 11 10.5	Jastrabá F. (Slovakia)	89 [50]	616 [50]	101 [50]
VSK 11 30.5	Jastrabá F. (Slovakia)	52 [50]	462 [50]	61 [50]
VSK 11 31.5	Jastrabá F. (Slovakia)	78 [50]	565 [50]	84 [50]
RO-M	Rokle (Czech Republic)	59 [49]	464 ± 5 [30]	57 ± 1 [49]
BM	Rokle (Czech Republic)	52 [51]	531 ± 6 [30]	62 [51]

The most interesting finding of this study is in the composition of exchangeable cations. Magnesium dominated bentonite lost a significant amount of exchangeable Mg^{2+} when heated. The proportion of Ca^{2+} and K^+ increased with heating, while Na^+ remained unaffected (see Figure 4). These changes in exchangeable cations took place in the solid state, without the influence of external fluids. In comparison, in the in situ experiments with access to groundwater, a gradually increasing proportion of the divalent cations towards the heater was observed [13]. Only water originally present in BCV_IN and escaping due to thermal loading could act as a transport medium. From this point of view, it is necessary to analyse the top layers of bentonite, which were excluded from

current research due to the small amount (see Section 2.1). The loss of exchangeable Mg^{2+} can be explained by increased fixation between charged surfaces [44] or crystal lattice transformation. Magnesium in the montmorillonite structure is located in the octahedral sheet together with Al and Fe [13]. It can be expected that when the montmorillonite lattice is damaged, Mg^{2+} is released from the structure, and the surface charge is redistributed. A very slight decrease in the mean layer charge density for montmorillonite was detected in compacted bentonite (Almeria, Spain) exposed in situ to 100 °C [52]. The change in surface charge density was deduced from our results of CEC, SSA and Cs sorption. Moreover, 1.5–2 times higher Mg concentrations were determined in the aqueous leachates from the thermally loaded samples compared to the input sample. Therefore, we are inclined to explain the changes in exchangeable cations to the partial lattice modifications. Plötze et al. [52], however, observed Mg enrichment in samples from the heater region, as in many large-scale tests [4,13]. The mechanism behind the Mg enrichment is not yet clear [4]. Both mechanisms, magnesium enrichment and depletion (as observed in this study), would be worth investigating thoroughly in future research.

The studied geotechnical parameters (free swelling, saturated hydraulic conductivity, and water retention curves) showed worsening with the thermal loading time. All these parameters are related to the behaviour of water in bentonite (maximal expansion of expandable structures in free swelling test, water uptake and transport through confined clay particles). As the water uptake ability of montmorillonite depends critically on the magnitude of the surface charge density of the particles [45], the observed geotechnical behaviour indicates changes in surface charge distribution. The resulting reduction of expandable clay structures towards low- or non-swelling clay structures upon heating was therefore subjected to data analysis of saturated hydraulic conductivity. Figure 9 displays hydraulic conductivities converted to a referential temperature of 10 °C, according to ISO 17892-11, for BCV bentonite and selected bentonites (from Table 6) tested by Karnland et al. [53]. A correlation between saturated hydraulic conductivity and montmorillonite content can be seen. The higher the k_{10}, the lower the montmorillonite content. The k_{10} values for BCV can be categorised between Rokle bentonite and Friedland clay, which corresponds well to their low montmorillonite content. The saturated hydraulic conductivity of Deponit CAN, MX-80 and Asha is one order of magnitude smaller due to higher montmorillonite content.
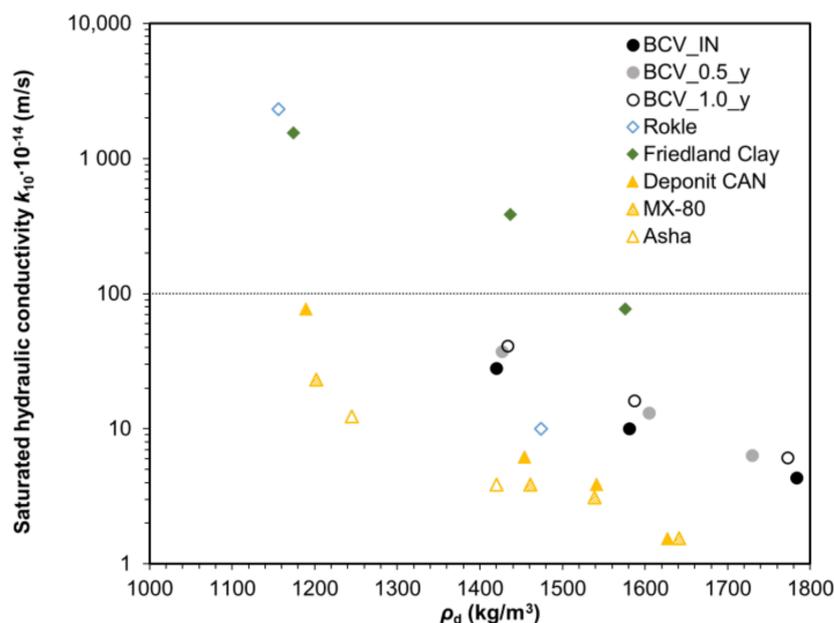
Figure 9. Saturated hydraulic conductivity of BCV compared to data for Friedland clay, Rokle, Deponit CAN, MX-80, and Asha [53].

A shift of measured saturated hydraulic conductivity for BCV towards clay material of lower montmorillonite content with thermal loading period can be clearly seen. Nevertheless, BCV meets an acceptance safety limit for saturated hydraulic conductivity of buffer lower than 10^{-12} m/s [17], even after the thermal loading. It can also be noticed in Figure 9 that the differences between input and thermally loaded BCV samples were more dramatic for lower dry densities, whereas for dry densities over 1700 kg/m^3, the differences induced by the thermal loading seem to be reduced. Based on this observation, it can be hypothesised that no significant effect of thermal loading on saturated hydraulic conductivity [13] might be due to the high density of bentonite samples. On the other hand, the most notable difference between BCV samples was found in free swelling tests, where the dry density was very low. Therefore, it seems that the thermally induced changes manifest more in less dense systems. For further investigation, higher dry densities or, and vice-versa, lower ones than those used (e.g., 2000 kg/m^3 and 1000 kg/m^3) would be promising to determine saturated hydraulic conductivity and WRC to highlight the impact of the thermal loading on buffer mass.

Water retention ability for all dry densities decreased with the thermal loading period. This behaviour was more relevant for lower water content; for water content above 20%, the water retention ability of both thermally unloaded and thermally loaded samples became closer to each other. This trend was also observed by [9]. The most significant difference is between the BCV_IN samples and the BCV_0.5_y ones; the difference between BCV_0.5_y and BCV_1.0_y is minor. It indicates that most of the material changes took place during the first half-year of thermal loading. This fact corresponds well with SSA values, where between BCV_IN and BCV_0.5_y, a crucial decrease was observed, whereas between BCV_0.5_y and BCV_1.0_y no visible change was detected.

Microbiological experiments under very hospitable conditions in a suspended state (i.e., without space and water availability limitation) with continuous electron donor supply in the form of H$_2$ present in an anaerobic atmosphere showed that heating of bentonite powder at 150 °C for up to one year did not result in bentonite sterilisation. However, a reduction of microbial load with increasing thermal loading time was observed. This reduction was especially true for the BCV_1.0_y samples, where microbial recovery was lower than BCV_IN and BCV_0.5_y. Our experiment further showed that microbial recovery from the dormant stages is a lengthy and probably partially stochastic procedure. After 14 days of cultivation, the signal in relative quantification seems to be rather random in the case of thermally loaded samples, while after 28 days of cultivation, the pattern was much more consistent, and this cultivation time proved to be more suitable for the detection of microbial activity restoration in bentonite samples at given environmental conditions.

Although we showed that bacteria could at least partially resume their activity after medium-term heat loading when cultivated at suitable conditions, the results imply that a substantial reduction in microbial load or even complete sterilisation of bentonite powder could be possible when the heating time exceeds one year. An equilibrium between an increase of the temperature limit at the canister surface resulting in bentonite sterilisation and the potential risk of losing favourable geochemical and geotechnical properties should therefore be addressed in the DGR performance assessment.

5. Conclusions

A medium-term thermal loading of bentonite powder resulted in detectable changes of properties, important directly or indirectly for the safety performance as a barrier material in a deep geological repository. No significant bentonite alteration, in terms of mineralogical composition, was observed by XRD. The thermal loading resulted in progressive disappearance of basal diffraction of montmorillonite, indicating increasing disorder of the montmorillonite layers. The impact of thermal loading on the overall bentonite composition was registered by aqueous leachates and TA-EGA mainly for carbonate phases, then for sulphates and fluorides.

Based on the determination of cation exchange capacity, total surface area and caesium distribution coefficient and interpretation of these parameters, it was concluded that montmorillonite had been partially altered in terms of the magnitude of the surface charge density of montmorillonite particles. Montmorillonite alteration towards low- or non-swelling clay structures was also supported by the determined geotechnical behaviour. Swelling ability and water uptake ability of thermally loaded samples were lower, and saturated hydraulic conductivity higher than for the input bentonite material.

This study has shown that XRD is a suitable method for mineralogical characterisation, but it was found to be insensitive for detecting slight variations of minerals in bentonite. In order to identify the altered montmorillonite fraction in more detail, a future investigation will focus on the clay fraction separation and its detailed analysis. We also plan to sample the heated bentonite powder after two years of thermal loading. Therefore, the current methods applied in this study to characterise bentonite properties will be amended to capture an alteration of clay minerals, especially by monitoring silica, aluminium, iron, and magnesium, which could confirm the hypothesis of thermal stress damage to the montmorillonite lattice.

The thermal loading also resulted in a reduction of microbial survivability and, thus, affected possible future microbial activity in bentonite. Thermal loading could play an important role in a permanent reduction of microbial activity in the bentonite buffer. However, more extended experiments focused on the stress-induced hindrances to microbial growth are needed.

References

1. Villar, M.V.; Armand, G.; Conil, N.; de Lesquen, C.; Herold, P.; Simo, E.; Mayor, J.C.; Dizier, A.; Li, X.; Chen, G.; et al. D7.1 HITEC. In *Initial State-of-the-Art on THM Behaviour of i) Buffer Clay Materials and of Ii) Host Clay Materials*; EURAD Project, Horizon: Brussels, Belgium, 2020; p. 222.
2. Leupin, O.X.; Birgersson, M.; Karnland, O.; Korkeakoski, P.; Sellin, P.; Mäder, U.; Wersin, P. *NAGRA Technical Report 14–12: Montmorillonite Stability under Near-Field Conditions*; National Cooperative for the Disposal of Radioactive Waste: Wettingen, Switzerland, 2014; p. 104.
3. Wersin, P.; Johnson, L.H.; McKinley, I.G. Performance of the bentonite barrier at temperatures beyond 100 °C: A critical review. *Phys. Chem. Earth Parts A/B/C* **2007**, *32*, 780–788. [CrossRef]
4. Kaufhold, S.; Dohrmann, R.; Ufer, K.; Svensson, D.; Sellin, P. Mineralogical analysis of bentonite from the ABM5 heater experiment at Äspö Hard Rock Laboratory, Sweden. *Minerals* **2021**, *11*, 669. [CrossRef]

5. Svensson, D.; Dueck, A.; Nilsson, U.; Olsson, S.; Sandén, T.; Lydmark, S.; Jägerwall, S.; Pedersen, K.; Hansen, S. SKB technical report TR-11-06: Alternative buffer material. In *Status of the Ongoing Laboratory Investigation of Reference Materials and Test Package 1.*; Swedish Nuclear Fuel and Waste Management Co: Stockholm, Sweden, 2011; p. 146.

6. Kumpulainen, S.; Kiviranta, L. *POSIVA Working Report 2011-41: Mineralogical and Chemical and Physical Study of Potential Buffer and Backfill Materials from ABM Test Package 1*; POSIVA Oy: Olkiluoto, Finland, 2011; p. 50.

7. Kumpulainen, S.; Kiviranta, L.; Korkeakoski, P. Long-term effects of an iron heater and äspö groundwater on smectite clays: Chemical and hydromechanical results from the in situ alternative buffer material (ABM) test package 2. *Clay Miner.* **2016**, *51*, 129–144. [CrossRef]

8. Villar, M.V.; Gutiérrez-Álvarez, C.; Martín, P.L. Low-suction water retention capacity of bentonite at high temperature. In *E3S Web of Conferences*; EDP Sciences: Les Ulis, France, 2020; Volume 195, p. 04010. [CrossRef]

9. Villar, M.V.; Gómez-Espina, R.; Lloret, A. Experimental investigation into temperature effect on hydro-mechanical behaviours of bentonite. *J. Rock Mech. Geotech. Eng.* **2010**, *2*, 71–78. [CrossRef]

10. Jacinto, A.C.; Villar, M.V.; Gómez-Espina, R.; Ledesma, A. Adaptation of the van Genuchten expression to the effects of temperature and density for compacted bentonites. *Appl. Clay Sci.* **2009**, *42*, 575–582. [CrossRef]

11. Cho, W.J.; Lee, J.O.; Chun, K.S. The temperature effects on hydraulic conductivity of compacted bentonite. *Appl. Clay Sci.* **1999**, *14*, 47–58. [CrossRef]

12. Daniels, K.A.; Harrington, J.F.; Zihms, S.G.; Wiseall, A.C. Bentonite permeability at elevated temperature. *Geosciences* **2017**, *7*, 3. [CrossRef]

13. Karnland, O.; Olsson, S.; Dueck, A.; Birgersson, M.; Nilsson, U.; Hernan-Håkansson, T.; Pedersen, K.; Nilsson, S.; Eriksen, T.E.; Rosborg, B. SKB technical report TR-09-29: Long term test of Buffer Material at the Äspö Hard Rock Laboratory, LOT Project. In *Final Report on the A2 Test. Parcel*; Svensk Kärnbränslehantering AB: Stockholm, Sweden, 2009; p. 279.

14. Van Humbeeck, H.; Verstricht, J.; Li, X.L.; De Cannière, P.; Bernier, F.; Kursten, B. *EURIDICE Report 09-134: The OPHELIE Mock-up Final Report*; EIG EURIDICE: Mol, Belgium, 2009; p. 197.

15. Fru, E.C.; Athar, R. In situ bacterial colonization of compacted bentonite under deep geological high-level radioactive waste repository conditions. *Appl. Microbiol. Biotechnol.* **2008**, *79*, 499–510. [CrossRef]

16. Enning, D.; Garrelfs, J. Corrosion of iron by sulfate-reducing bacteria: New views of an old problem. *Appl. Environ. Microbiol.* **2014**, *80*, 1226–1236. [CrossRef] [PubMed]

17. Andersson, J.; Vira, J.; Salo, J.-P.; Morén, L.; Pers, K.; Pastina, B.; Hellä, P. *Posiva SKB Report 01: Safety Functions, Performance Targets and Technical Design Requirements for a KBS-3V Repository*; Svensk Kärnbränslehantering AB: Forsmark, Sweden; Posiva Oy: Eurajoki, Finland, 2017; p. 120.

18. Nicholson, W.L.; Munakata, N.; Horneck, G.; Melosh, H.J.; Setlow, P. Resistance of bacillus endospores to extreme terrestrial and extraterrestrial environments. *Microbiol. Mol. Biol. Rev.* **2000**, *64*, 548–572. [CrossRef]

19. Setlow, P. Spores of bacillus subtilis: Their resistance to and killing by radiation, heat and chemicals. *J. Appl. Microbiol.* **2006**, *101*, 514–525. [CrossRef]

20. Masurat, P.; Eriksson, S.; Pedersen, K. Microbial sulphide production in compacted wyoming bentonite MX-80 under in situ conditions relevant to a repository for high-level radioactive waste. *Appl. Clay Sci.* **2010**, *47*, 58–64. [CrossRef]

21. Masurat, P.; Eriksson, S.; Pedersen, K. Evidence of Indigenous sulphate-reducing bacteria in commercial wyoming bentonite MX-80. *Appl. Clay Sci.* **2010**, *47*, 51–57. [CrossRef]

22. Bengtsson, A.; Pedersen, K. Microbial sulphide-producing activity in water saturated wyoming MX-80, asha and calcigel bentonites at wet densities from 1500 to 2000 Kg M−3. *Appl. Clay Sci.* **2017**, *137*, 203–212. [CrossRef]

23. Bengtsson, A.; Pedersen, K. Microbial sulphate-reducing activity over load pressure and density in water saturated boom clay. *Appl. Clay Sci.* **2016**, *132–133*, 542–551. [CrossRef]

24. Hausmannová, L.; Hanusová, I.; Dohnálková, M. *SÚRAO Technical Report 309/2018: Summary of the Research of Czech Bentonites for Use in the Deep Geological Repository-Up To 2018*; Správa úložišť radioaktivních odpadů: Praha, Czech Republic, 2018; p. 63.

25. Doebelin, N.; Kleeberg, R. Profex: A graphical user interface for the rietveld refinement program BGMN. *J. Appl. Cryst.* **2015**, *48*, 1573–1580. [CrossRef]

26. Meier, L.P.; Kahr, G. Determination of the cation exchange capacity (CEC) of clay minerals using the complexes of copper (II) ion with triethylenetetramine and tetraethylenepentamine. *Clays Clay Miner.* **1999**, *47*, 386–388. [CrossRef]

27. Ammann, L.; Bergaya, F.; Lagaly, G. Determination of the cation exchange capacity of clays with copper complexes revisited. *Clay Miner.* **2005**, *40*, 441–453. [CrossRef]

28. Carter, D.L.; Heilman, M.D.; Gonzales, C.L. Ethylene glycol monoethyl ether for determining surface area of silicate minerals. *Soil Sci.* **1965**, *100*, 356–360. [CrossRef]

29. Carter, D.L.; Mortland, M.M.; Kemper, W.D. Specific Surface. In *Methods of Soil Analysis*; John Wiley & Sons: Hoboken, NJ, USA, 1986; pp. 413–423. ISBN 978-0-89118-864-3.

30. Brázda, L.; Červinka, R. Determination of specific surface area of clay minerals by EGME method. In Proceedings of the 4th BELBaR Annual Workshop, Berlin, Germany, 15 September 2016.

31. ASTM. *D5890-19 Test Method for Swell Index of Clay Mineral Component of Geosynthetic Clay Liners*; ASTM International: West Conshohocken, PA, USA, 2019.

32. Gondolli, J.; Večerník, P. The uncertainties associated with the application of through-diffusion, the steady-state method: A case study of strontium diffusion. *Geol. Soc. Spec. Publ.* **2014**, *400*, 603–612. [CrossRef]
33. Villar, M.V. Water retention of two natural compacted bentonites. *Clays Clay Miner.* **2007**, *55*, 311–322. [CrossRef]
34. Černoušek, T.; Shrestha, R.; Kovářová, H.; Špánek, R.; Ševců, A.; Sihelská, K.; Kokinda, J.; Stoulil, J.; Steinová, J. Microbially influenced corrosion of carbon steel in the presence of anaerobic sulphate-reducing bacteria. *Corros. Eng. Sci. Technol.* **2019**, *55*, 127–137. [CrossRef]
35. Filipská, P.; Zeman, J.; Všianský, D.; Honty, M.; Škoda, R. Key Processes of long-term bentonite-water interaction at 90 °C: Mineralogical and chemical transformations. *Appl. Clay Sci.* **2017**, *150*, 234–243. [CrossRef]
36. Sasaki, Y.; Shibata, M.; Yui, M.; Ishikawa, H. Experimental Studies on the Interaction of Groundwater with Bentonite. *MRS Online Proc. Libr.* **1995**, *353*, 337–344. [CrossRef]
37. Vejsada, J.; Hradil, D.; Řanda, Z.; Jelínek, E.; Štulík, K. Adsorption of cesium on czech smectite-rich clays—A comparative study. *Appl. Clay Sci.* **2005**, *30*, 53–66. [CrossRef]
38. Černá, K.; Černoušek, T.; Polívka, P.; Ševců, A. Survival of Microorganisms in Bentonite Subjected to Different Levels of Irradiation and Pressure. In Proceedings of the Microbiology in Nuclear Waste Disposal, Stockholm, Sweden, 7–9 May 2019; p. 57, No 661880.
39. Steudel, A.; Mehl, D.; Emmerich, K. Simultaneous thermal analysis of different bentonite–sodium carbonate systems: An attempt to distinguish alkali-activated bentonites from raw materials. *Clay Miner.* **2013**, *48*, 117–128. [CrossRef]
40. Kaufhold, S.; Emmerich, K.; Dohrmann, R.; Steudel, A.; Ufer, K. Comparison of Methods for Distinguishing Sodium Carbonate Activated from Natural Sodium Bentonites. *Appl. Clay Sci.* **2013**, *86*, 23–37. [CrossRef]
41. García-Romero, E.; Lorenzo, A.; García-Vicente, A.; Morales, J.; García-Rivas, J.; Suárez, M. On the structural formula of smectites: A review and new data on the influence of exchangeable cations. *J. Appl Cryst.* **2021**, *54*, 251–262. [CrossRef] [PubMed]
42. Thomas, J.; Glass, H.D.; White, W.A.; Trandell, R.M. Flouride content of clay minerals and argillaceous earth materials. *Clays Clay Miner.* **1977**, *25*, 278–284. [CrossRef]
43. Kale, R.C.; Ravi, K. Influence of thermal loading on index and physicochemical properties of barmer bentonite. *Appl. Clay Sci.* **2018**, *165*, 22–39. [CrossRef]
44. Kaufhold, S.; Dohrmann, R. Effect of extensive drying on the cation exchange capacity of bentonites. *Clay Miner.* **2010**, *45*, 441–448. [CrossRef]
45. Birgersson, M.; Hedström, M.; Karnland, O.; Sjöland, A. Chapter 12-bentonite buffer: Macroscopic performance from nanoscale properties. In *Geological Repository Systems for Safe Disposal of Spent Nuclear Fuels and Radioactive Waste*; Woodhead Publishing: Duxford, UK, 2017; ISBN 978-0-08-100652-8.
46. Chipera, S.J.; Bish, D.L. Baseline studies of the clay minerals society source clays: Powder X-ray diffraction. *Clays Clay Miner.* **2001**, *49*, 398–409. [CrossRef]
47. Borden, D.; Giese, R.F. Baseline studies of the clay minerals society source clays: Cation Exchange capacity measurements by the ammonia-electrode method. *Clays Clay Miner.* **2001**, *49*, 444–445. [CrossRef]
48. Fernandez, A.M.; Cuevas, J.; Rivas, P. Pore water chemistry of the febex bentonite. In Proceedings of the Scientific Basis for Nuclear Waste Management XXIV: Materials Research Society Symposium Proceedings, Sydney, Australia, 27–31 August 2000; Volume 663. [CrossRef]
49. Vejsada, J. The uncertainties associated with the application of batch technique for distribution coefficients determination—A case study of cesium adsorption on four different bentonites. *Appl. Radiat. Isot.* **2006**, *64*, 1538–1548. [CrossRef] [PubMed]
50. Osacký, M.; Binčík, T.; Paľo, T.; Uhlík, P.; Madejová, J.; Czímerová, A. Mineralogical and Physico–Chemical Properties of Bentonites from the Jastrabá Formation (Kremnické Vrchy Mts., Western Carpathians). *Geol. Carpathica* **2019**, *70*, 433–445. [CrossRef]
51. Vejsada, J.; Jelínek, E.; Řanda, Z.; Hradil, D.; Přikryl, R. Sorption of cesium on smectite-rich clays from the bohemian massif (Czech Republic) and their mixtures with sand. *Appl. Radiat. Isot.* **2005**, *62*, 91–96. [CrossRef]
52. Plötze, M.; Kahr, G.; Dohrmann, R.; Weber, H. Hydro-mechanical, geochemical and mineralogical characteristics of the bentonite buffer in a heater experiment: The HE-B project at the Mont Terri Rock laboratory. *Phys. Chem. Earth Parts A/B/C* **2007**, *32*, 730–740. [CrossRef]
53. Karnland, O.; Olsson, S.; Nilsson, U. *SKB Technical Report TR-06-30: Mineralogy and Sealing Properties of Various Bentonites and Smectite-Rich Clay Materials*; Svensk Kärnbränslehantering AB: Stockholm, Sweden, 2006; p. 112.